



## Vanishing Fe 3d orbital moments in single-crystalline magnetite

To cite this article: E. Goering *et al* 2006 *EPL* **73** 97

View the [article online](#) for updates and enhancements.

### You may also like

- [Evolution of electronic and magnetic properties of nominal magnetite nanoparticles at high pressure probed by x-ray absorption and emission techniques](#)  
Kalpani Werellapatha, Carlos A Escanhoela, Gilberto Fabbri et al.
- [Relation between spin and orbital magnetism in excited states of ferromagnetic materials](#)  
L M Sandratskii
- [On the 'centre of gravity' method for measuring the composition of magnetite/maghemite mixtures, or the stoichiometry of magnetite-maghemite solid solutions, via  \$^{57}\text{Fe}\$  Mössbauer spectroscopy](#)  
Jeppe Fock, Lara K Bogart, David González-Alonso et al.

## Vanishing Fe 3d orbital moments in single-crystalline magnetite

E. GOERING, S. GOLD, M. LAFKIOTI and G. SCHÜTZ

*Max-Planck-Institut für Metallforschung - Heisenbergstrasse 3  
70569 Stuttgart, Germany*

received 2 August 2005; accepted in final form 2 November 2005

published online 7 December 2005

PACS. 75.47.-m – Magnetotransport phenomena; materials for magnetotransport.

PACS. 78.70.Dm – X-ray absorption spectra.

PACS. 71.30.+h – Metal-insulator transitions and other electronic transitions.

**Abstract.** – We show detailed magnetic absorption spectroscopy results of an *in situ* cleaved high-quality single crystal of magnetite. In addition the experimental setup was carefully optimized to reduce drift, self-absorption, and offset phenomena as far as possible. In strong contradiction to recently published data, our observed orbital moments are nearly vanishing and the spin moments are quite close to the integer values proposed by theory. This very important issue supports the half-metallic full-spin-polarized picture of magnetite.

*Introduction.* – Magnetite  $\text{Fe}_3\text{O}_4$  has been fascinating mankind for thousands of years [1].  $\text{Fe}_3\text{O}_4$  shows a phase transition, the so-called Verwey transition at  $T_V \approx 123$  K, accompanied with a jump in the electrical conductivity, which has been extensively investigated in the last century (for a review see refs. [2] or [3] and references therein). Today magnetite has attracted enormous interest, because of the proposed high spin polarization and related possible applications for future spin electronic devices [4]. The nature of the conducting electrons and the influence of local electronic correlations are one of the key issues to understand  $\text{Fe}_3\text{O}_4$  [5].  $\text{Fe}_3\text{O}_4$  crystallizes at room temperature in the antiferromagnetic cubic inverse Spinel structure ( $Fd\bar{3}m$ ), formally written as  $\text{Fe(A)Fe(B)}_2\text{O}_4$  [6]. The A-type ions are tetrahedrally coordinated and nominally in a  $\text{Fe}^{3+}$  ( $\approx -5\mu_B$ ) configuration. The B-site ions are located on octahedral sites and mixed valent with equally distributed  $\text{Fe}^{3+}$  ( $\approx +5\mu_B$ ) and  $\text{Fe}^{2+}$  ( $\approx +4\mu_B$ ) ions. The magnetic moments shown in brackets are pure spin moments related to a fully occupied local majority band (opposite for A and B sites). The magnetic moments of the A and B sites are aligned antiparallel to each other with a resulting magnetization per formula unit  $5\mu_{B(B)} + 4\mu_{B(B)} - 5\mu_{B(A)} = 4\mu_B$ , consistent to the experimental result of  $4.07\mu_B$  [7]. An observation of an integer spin moment is therefore a clear indication for a B-site minority electron conduction mechanism, and its accompanied full spin polarization at the Fermi level. The phase transition at  $T_V = 123$  K has been explained by Verwey in terms of a charge localization-delocalization of the conducting B-site electrons [8–10]. This discussion is recently revived experimentally and theoretically by refined structural data results [11–13], which found only a slightly corrugated charge order between 2.4–2.6e, accompanied by orbital ordering [13, 14].

In a recent letter [15] the spin and orbital Fe 3d magnetic moments of magnetite have been evaluated experimentally by X-ray magnetic circular dichroism (XMCD) and calculated within the LDA+U scheme using a rotationally invariant LDA+U functional. Non-integer spin moments and large unquenched B-site orbital moments of  $0.33\mu_B$  have been found, which have been attributed to a strong onsite Coulomb interaction and corresponding 3d correlation effects. Other reported band structure calculations and LDA+U calculations, using the original LDA+U functional, found only small orbital moments, and the Fe spin moments were just slightly reduced from the integer value due to hybridization with O [5, 16–18].

In this contribution, we will show carefully performed XMCD experiments, which are consistent to the majority of theoretical predictions [5, 16–18], confirming the integer moment description and the full-spin-polarized model of  $\text{Fe}_3\text{O}_4$  with a very small integral orbital moment. The extracted sum rule [19, 20] related spin and orbital moments are therefore in contradiction to ref. [15]. To clearly point out the quality and validity of our results, we will discuss in detail the experimental procedure and possible experimental error sources, like surface effects, signal drift, self-absorption, and offset phenomena. The chosen experimental setup has been optimized to minimize these error sources as far as possible.

*Experimental.* – All XMCD spectra have been measured in total electron yield mode (TEY) at the BESSY II bending magnet beamline PM3 in an applied magnetic field of 10 kOe, providing full sample saturation at all temperatures. All sum rule related values have been corrected for the finite circular polarization of  $0.93\pm 0.02$ . The absorption has been normalized to the incoming photon beam intensity by measuring synchronously the photocurrent of a gold grid. To prevent even very small non-XMCD-related current asymmetries, normal-incidence conditions have been used and the sample was biased at  $-100\text{ V}$  to minimize magnetic-field-induced electron backscattering phenomena [21]. Our raw data “XMCD-like-offset”, which is not related to the intrinsic magnetic properties of the sample, was smaller than 1/1000 of the total absorption. But even this very small residual XMCD-like-offset, monitored at energies below 690 eV, has been numerically treated and subtracted. This procedure and the physics behind the “XMCD-like-offset” have been described in detail elsewhere [21].

The sample magnetization has been flipped at every data point to compensate even for smallest synchrotron-related drift phenomena. In addition, the results have been verified for opposite light helicity. The monochromator energy resolution was set to  $\approx 6000$ . High-quality synthetic single-crystalline samples have been prepared by Brabers in an arc-image furnace using the floating-zone technique [22]. Single crystals have been annealed and cooled under equilibrium conditions to obtain highly stoichiometric single crystals [23]. The vacancy concentration of the used  $\text{Fe}_{3-x}\text{O}_4$  single crystal is smaller than  $x < 10^{-6}$ , proven by measuring magnetic after-effect spectra [2, 24]. As derived from SQUID measurements, the Verwey temperature of the single crystal is  $T_V = 124\text{ K}$ . The single crystal has been *in situ* cleaved at room temperature (surface normal along [110]-direction), at an ambient pressure smaller than  $10^{-9}\text{ mBar}$ .

We would like to emphasize that our cleaved sample has shown —during the same synchrotron measurement time— a sharp shift of the O K edge onset monitoring the gap variation at the Verwey transition [25]. This demonstrates that the shown absorption results of the cleaved single crystal used here, exhibit bulk properties of magnetite. This is also consistent to recently published high-energy photoemission results [26].

A typical XAS and XMCD spectrum is shown in fig. 1a. The general shape of the XAS lines is comparable to the results presented in ref. [15]. The integrated XMCD signal (fig. 1b) exhibits a non-vanishing slope between 730–765 eV, which is related to a very small and reproducible XMCD signal above the  $L_2$  edge region.

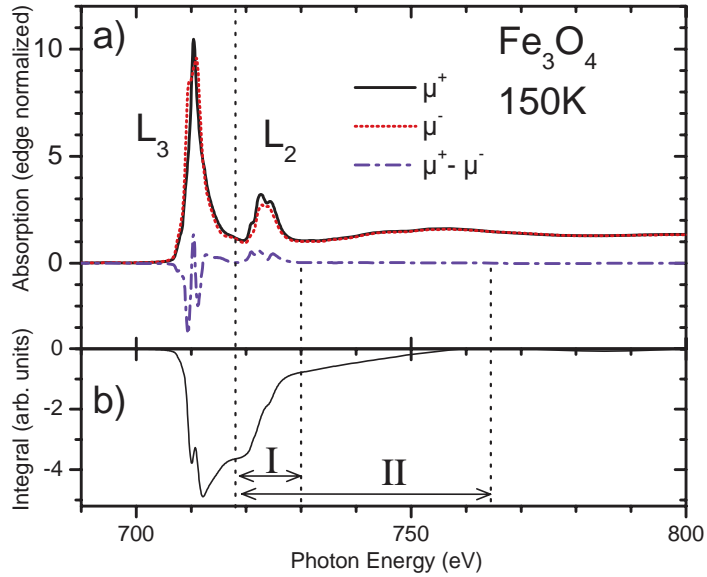


Fig. 1 – a) X-ray absorption and XMCD spectrum of a fractured single crystal of magnetite at 150 K and normal-incidence geometry. b) Integrated XMCD spectrum used for sum rule analysis. Different sum rule integration ranges are indicated as I and II.

Sum rules [19, 20] have been applied for two different L<sub>2</sub> edge integration ranges (range I: 718–730 eV and range II: 718–764.5 eV) to show the influence of this small high-energy XMCD signal. The background intensity has been subtracted in a standard way, with L<sub>3</sub> (L<sub>2</sub>) edge centre position at 710.7 eV (723.3 eV) [27], and the same number of Fe 3d holes  $N_h/\text{Fe} = 13.5/3$  has been used as in ref. [15]. Results are shown in fig. 2. For the orbital moments the estimated error bar is about the symbol height. Only minor temperature dependencies are observable, comparable to SQUID-related magnetization curves. An important point is the absence of prominent difference between above and below the Verwey transition. The average orbital moments are  $-0.001\mu_B$  ( $0.06\mu_B$ ) for the extended (short) integration range. The obtained maxi-

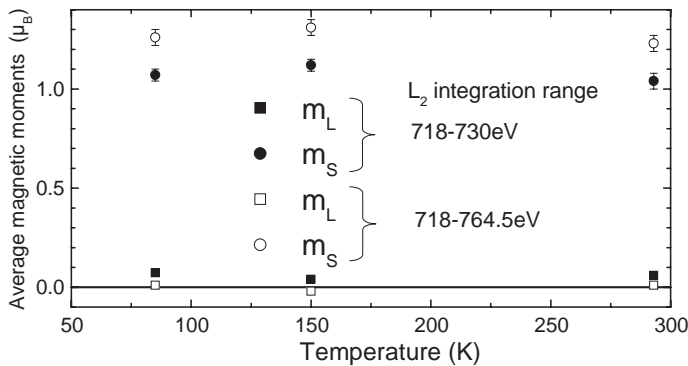


Fig. 2 – Spin and orbital magnetic moments, determined for a short and extended integration range at different temperatures (see text).

mal sum rule related effective spin moment/FU is  $(m_s + 7\langle T_z \rangle) = 3 \cdot 1.30\mu_B = 3.90 \pm 0.09\mu_B$  (long range). We would like to emphasize, that sum rules only give an average information over the whole formula unit of all three Fe ions.

*Discussion.* – The necessity of using such a long integration range can be explained by the presence of magnetic extended fine-structure (MEXAFS) oscillations at the  $L_{2,3}$  edges, which are always superimposed to the resonant XMCD structure [28, 29]. Therefore, some part of the  $L_3$  edge MEXAFS is superimposed to the  $L_2$  edge signal. This modifies sum rule values with short integration range. Due to the fact that the MEXAFS signal is strongly damped at higher excitation energies, the dominating parts of the  $L_3$  and  $L_2$  edges, close to the excitation threshold, have opposite sign and cancel each other [29] for extended integration ranges. A similar relative strong MEXAFS-related intensity has been identified for  $\text{CrO}_2$ , another ferromagnetic oxide [30].

The observed nearly vanishing orbital moment is consistent to the pure LDA calculation in ref. [15] and to other theoretical approaches [5, 16–18]. The effective spin moment/FU of  $(m_s + 7\langle T_z \rangle) = 3.90 \pm 0.09\mu_B$  is much larger than the uncorrected LDA+U value of  $3.2\mu_B$  from ref. [15], but in perfect agreement with the calculation of Penicaud *et al.* [17], and quite close to other reference values [5, 16, 18]. The result presented here exhibits a nearly integer spin value per formula unit and supports the full-spin-polarized picture of magnetite as introduced above. Due to the predominantly cubic symmetry, even below  $T_V$ , and because of the consistency of our results, we do not believe that  $T_z$  plays an important role in our measurements [31]. The magnetic dipole term  $\langle T_z \rangle$  is only present for systems with symmetry less than cubic [31]. To exclude additional surface symmetry breaking effects and related  $\langle T_z \rangle$  contributions, we have performed angular-dependent effective spin moment measurements for a polished magnetite sample (not shown), but no variations, *i.e.*  $\langle T_z \rangle$  influences, have been found. Therefore, we can conclude that the magnetic dipole term  $\langle T_z \rangle$  is quite small, and does not result in significant effective spin contributions.

At this point we will quantitatively discuss saturation effects, to make obvious the validity of our results. In the past Gota *et al.* have investigated  $\text{Fe}_3\text{O}_4$  TEY mode saturation effects for a thin-film sample as a function of the angle of incidence and sample thickness [32], where an unusual large value of  $\lambda_e = 5$  nm has been found, which is about 2–7 times larger compared to other published effective electron escape length values [33–36].

Therefore, we have performed angular-dependent XAS measurements on a polished [111]  $\text{Fe}_3\text{O}_4$  surface, from a fracture of the single crystal discussed above. Figure 3 shows a long energy range normal-incidence spectrum, which is carefully adapted to the Henke table atomic absorption curves for  $\text{Fe}_3\text{O}_4$  [37, 38]. The determined resonant absorption length scales are quite similar but also slightly reduced, compared to the absorption published by Gota *et al.* [32]. This reduction, not significant for the conclusions given here, is related to the extended adaptation range, which we have used to reduce errors related to the oscillating region between 730 and 780 eV [33].

Figure 4a shows the Fe  $L_{2,3}$  edge region of the Henke-table-adapted non-magnetic absorption lines for normal ( $0^\circ$ ) and  $60^\circ$  angle of incidence. Only very small differences are observable at high absorption values near 710 eV. This region is magnified in fig. 4b for  $0^\circ$ ,  $45^\circ$ , and  $60^\circ$  angles of incidence. We corrected these absorption coefficients for self-absorption (fig. 4c), choosing an effective electron escape length of  $\lambda_e = 0.8 \pm 0.3$  nm [35], in order to achieve best agreement between the corrected angular-dependent curves. This single-crystal-related effective electron escape length is much smaller compared to the  $\lambda_e = 5$  nm thin-film result [32]. A very similar value of 0.7 nm has been previously determined for another oxide system:  $\text{CrO}_2$  [33].

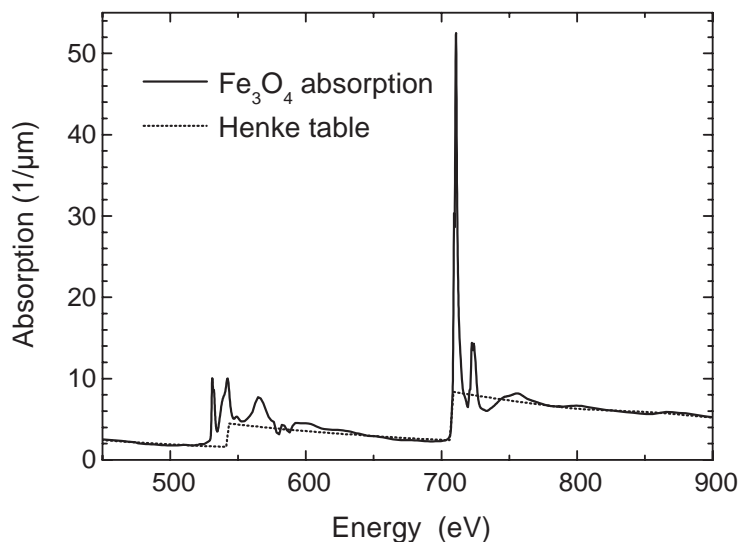


Fig. 3 –  $\text{Fe}_3\text{O}_4$  non-magnetic normal-incidence TEY signal adapted and compared to the Henke table tabulated absorption [35].

The total peak height variation induced by saturation effects is about 3% (5.4%) for the normal-incidence ( $60^\circ$ ) spectrum (difference between fig. 4b and c). Due to the oscillating behaviour of the  $L_3$  edge XMCD the influence on the orbital moment is even smaller. In case of the fractured single-crystal result at normal incidence, the orbital-moment saturation correction is smaller than  $0.01\mu_B$ . In order to check the maximum influence of the saturation effects, we have additionally calculated the orbital-moment variation for the large escape length

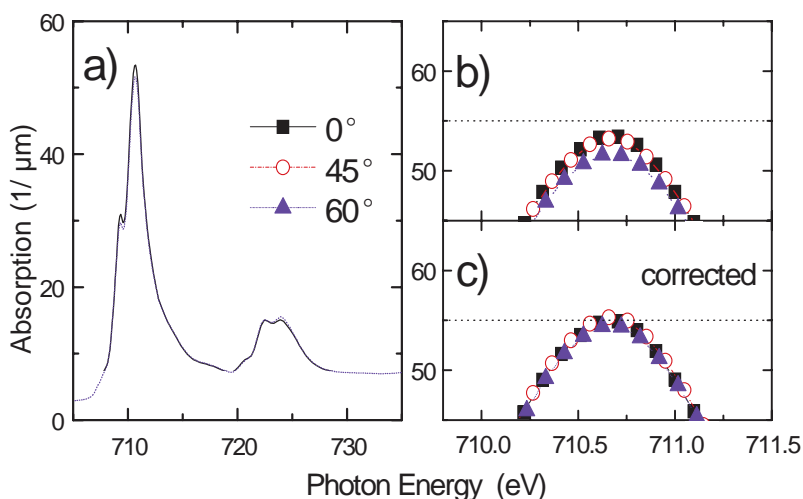


Fig. 4 – a) Angular-dependent non-magnetic Henke-table-adapted TEY spectra of a polished single crystal. Maximal self-absorption effects are shown in an expanded view: Uncorrected (b) and corrected (c).

$\lambda_e = 5 \text{ nm}$  [32], where the orbital-moment shift is only  $0.05\mu_B$ . The determined orbital moment per B-site is therefore less than  $3/2 * 0.01\mu_B = 0.015\mu_B$  (even for  $\lambda_e = 5 \text{ nm}$  smaller than  $0.08\mu_B$ ). The different escape length between this contribution and the results from Gota *et al.* can be in principle related to different surface roughness parameters, where roughness gives rise to an effective variation of the angle of incidence. On the other hand, open micro (or nano) trenches could also be responsible for an enhanced effective electron escape length. Up to now this has not been investigated on a quantitative basis. Due to the lack of surface-related information, we will not discuss the difference between both escape length estimations. It is outside the scope of this contribution to discuss all other possible explanations for the observed differences in the effective electron escape length, for example electrical-conductivity variations.

Nevertheless, we have clearly shown that for normal-incidence geometry saturation effects do not significantly modify our XMCD results, even for the large electron escape length values from Gota *et al.* Our results demonstrate the necessity to obtain high-quality wide-range XMCD data for  $\text{Fe}_3\text{O}_4$  to extract correct orbital-moment values. However, even for the short integration range the orbital moment is far below the values presented in ref. [15]. The origin of this difference is most likely not related to the physics of  $\text{Fe}_3\text{O}_4$ , and will be discussed in more detail elsewhere [39].

*Conclusion.* – In conclusion, our carefully performed experimental XMCD results for magnetite are in very good agreement with the majority of theoretical investigations. Self-absorption and other experimental effects have been neglected as a possible source of significant XMCD-related moment variation, especially for the orbital moment. Taking into account an extended XMCD integration range gives a magnetic spin moment, quite close to the expected integer value of  $4\mu_B$ , while the orbital moment vanishes. This result clearly supports the full-spin-polarized picture of magnetite.

\* \* \*

We thank M. FÄHNLE, F. WALZ, and H. KRONMÜLLER for fruitful discussions, and the Max-Planck-Society for financial support. Many thanks to V.A.M. BRABERS providing the magnetite sample and T. KACHEL from BESSY II for support during the beamtime.

## REFERENCES

- [1] MATTIS D. C., *The Theory of Magnetism I* (Springer, Berlin) 1988.
- [2] WALZ F., *J. Phys. Condens. Matter*, **14** (2002) R285.
- [3] GARCIA J. and SUBIAS G., *J. Phys. Condens. Matter*, **16** (2004) R145.
- [4] COEY J. M. D., VERSLUIS J. J. and VENKATESAN M., *J. Phys. D*, **35** (2002) 2457.
- [5] ZHANG ZE. and SATPATHY S., *Phys. Rev. B*, **44** (1991) 13319.
- [6] ANDERSON P. W., *Phys. Rev.*, **102** (1956) 1008.
- [7] WEISS P. and FORRER R., *Ann. Phys. (Paris)*, **12** (1929) 279.
- [8] VERWEY E. J. W., *Nature*, **144** (1939) 327.
- [9] VERWEY E. J. W. and HAAYMAN P. W., *Physica*, **8** (1941) 979.
- [10] VERWEY E. J. W., HAAYMAN P. W. and ROMELJN F. C., *J. Chem. Phys.*, **15** (1947) 181.
- [11] WRIGHT J. P., ATTFIELD J. P. and RADAELLI P. G., *Phys. Rev. Lett.*, **87** (2001) 266401-1.
- [12] WRIGHT J. P., ATTFIELD J. P. and RADAELLI P. G., *Phys. Rev. B*, **66** (2002) 214422-1.
- [13] LEONOV I., YARESKO A. N., ANTONOV V. N., KOROTIN M. A. and ANISIMOV V. I., *Phys. Rev. Lett.*, **93** (2004) 146404-1.
- [14] JENG H. T., GUO G. Y. and HUANG D. J., *Phys. Rev. Lett.*, **93** (2004) 156403-1.
- [15] HUANG D. J., CHANG C. F., JENG H. T., GUO G. Y., LIN H. J., WU W. B., KU H. C., FUJIMORI A., TAKAHASHI Y. and CHEN C. T., *Phys. Rev. Lett.*, **93** (2004) 077204-1.

- [16] ANTONOV V. N., HARMON B. N. and YARESKO A. N., *Phys. Rev. B*, **67** (2003) 024417-1.
- [17] PENICAUD M., SIBERCHICOT B., SOMMERS C. B. and KÜBLER J., *J. Magn. & Magn. Mater.*, **103** (1992) 212.
- [18] YANASE A. and SIRATORI K., *J. Phys. Soc. Jpn.*, **53** (1984) 312.
- [19] CARRA P., THOLE B. T., ALTARELLI M. and WANG X., *Phys. Rev. Lett.*, **70** (1993) 694.
- [20] THOLE B. T., CARRA P., SETTE F. and VAN DER LAAN G., *Phys. Rev. Lett.*, **68** (1992) 1943.
- [21] GOERING E., GOLD S., BAYER A. and SCHÜTZ G., *J. Synchrotron Radiat.*, **8** (2001) 434.
- [22] BRABERS V. A. M., *J. Cryst. Growth*, **8** (1971) 26.
- [23] KUIPERS A. J. M. and BRABERS V. A. M., *Phys. Rev. B*, **14** (1976) 1401.
- [24] WALZ F., BRABERS V. A. M., CHIKAZUMI S., KRONMÜLLER H. and RIGO M. O., *Phys. Status Solidi B*, **110** (1982) 471.
- [25] GOERING E., GOLD S., LAFKIOTI M., SCHÜTZ G. and BRABERS V. A. M., *Phys. Rev. B*, **72** (2005) 033112-1.
- [26] SCHRUPP D., SING M., TSUNCKAWA M., FUJIWARA H., KASAI S., SEKIYAMA A., SUGA S., MURO T., BRABERS V. A. M. and CLAESSEN R., *Europhys. Lett.*, **70** (2005) 789.
- [27] CHEN C. T., IDZERDA Y. U., LIN H. J., SMITH N. V., MEIGS G., CHABAN E., HO G. H., PELLEGRIN E. and SETTE F., *Phys. Rev. Lett.*, **75** (1995) 152.
- [28] LEMKE L., WENDE H., SRIVASTAVA P., CHAUVISTRE R., HAAK N., BABERSCHKE K., HUNTER-DUNN J., ARVANITIS D., MARTENSSON N., ANKUDINOV A., and REHR J. J., *J. Phys. Condens. Matter*, **10** (1998) 1917.
- [29] AHLERS D., ATTENKOFER K., and SCHÜTZ G., *J. Appl. Phys.*, **83** (1998) 7085.
- [30] GOERING E., BAYER A., GOLD S., SCHÜTZ G., RABE M., RÜDIGER U., and GÜNTHERODT G., *Phys. Rev. Lett.*, **88** (2002) 207203-1.
- [31] STÖHR J. and KÖNIG H., *Phys. Rev. Lett.*, **75** (1995) 3748.
- [32] GOTA S., GAUTIER-SOYER M. and SACCHI M., *Phys. Rev. B*, **62** (2000) 4187.
- [33] GOERING E., JUSTEN M., GEISSLER J., RÜDIGER U., RABE M., GÜNTHERODT G. and SCHÜTZ G., *Appl. Phys. A*, **74** (2002) 747.
- [34] HUNTER-DUNN J., ARVANITIS D., MARTENSSON N., TISCHER M., MAY F., RUSSO M. and BABERSCHKE K., *J. Phys. Condens. Matter*, **7** (1995) 1111.
- [35] NAKAJIMA R., STÖHR J. and IDZERDA Y. U., *Phys. Rev. B*, **59** (1999) 6421.
- [36] WILHELM F., POULOPOULOS P., SHRIVASTAVA P., WENDE H., FARLE M., BABERSCHKE K., ANGELAKERIS M., FLEVARIS N. K., GRANGE W., KAPPLER J. P., GHIRINGHELLI G. and BROOKES N. B., *Phys. Rev. B*, **61** (2000) 8647.
- [37] HENKE B. L., GULLIKSON E. M. and DAVIS J. C., *Center of X-ray Optics LBNL*, (2002) .
- [38] HENKE B. L., GULLIKSON E. M. and DAVIS J. C., *At. Data Nucl. Data Tables*, **54** (1993) 181.
- [39] GOERING E., LAFKIOTI M. and GOLD S., submitted to *Phys. Rev. Lett.* (2005).